STREAMING VISUAL GEOMETRY TRANSFORMER

Anonymous authors

Paper under double-blind review

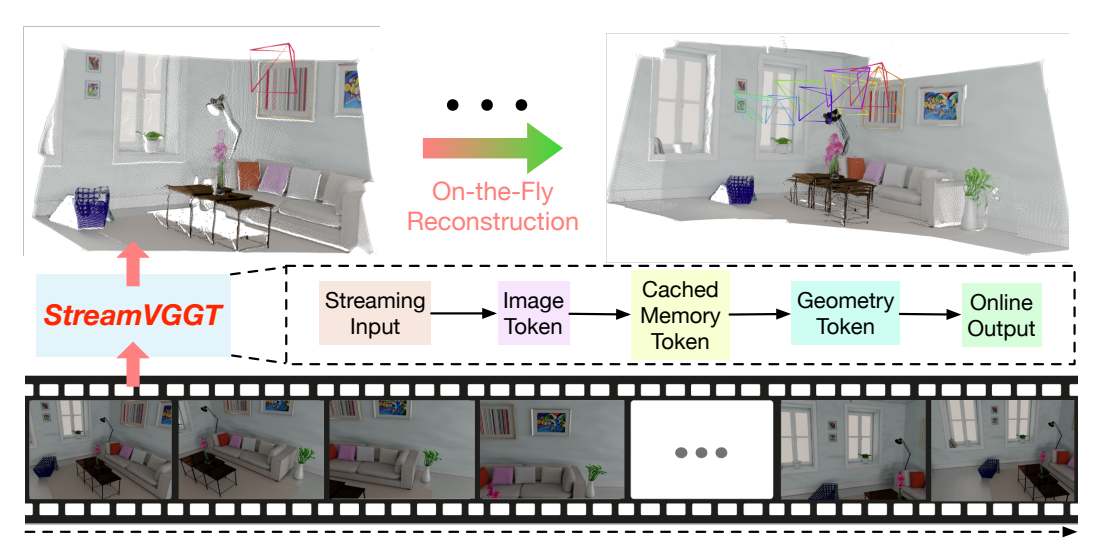


Figure 1: **Overview.** Unlike offline models that require reprocessing the entire sequence and reconstructing the entire scene upon receiving each new image, our StreamVGGT employs temporal causal attention and leverages cached token memory to support efficient incremental on-the-fly reconstruction, enabling interactive and low-latency online applications.

ABSTRACT

Perceiving and reconstructing 3D geometry from videos is a fundamental yet challenging computer vision task. To facilitate interactive and low-latency applications, we propose a streaming visual geometry transformer that shares a similar philosophy with autoregressive large language models. We explore a simple and efficient design and employ a causal transformer architecture to process the input sequence in an online manner. We use temporal causal attention and cache the historical keys and values as implicit memory to enable efficient streaming long-term 3D reconstruction. This design can handle low-latency 3D reconstruction by incrementally integrating historical information while maintaining high-quality spatial consistency. For efficient training, we propose to distill knowledge from the dense bidirectional visual geometry grounded transformer (VGGT) to our causal model. For inference, our model supports the migration of optimized efficient attention operators (e.g., FlashAttention) from large language models. Extensive experiments on various 3D geometry perception benchmarks demonstrate that our model enhances inference speed in online scenarios while maintaining competitive performance, thereby facilitating scalable and interactive 3D vision systems.

1 Introduction

3D geometry reconstruction has long been a fundamental task in computer vision (Hartley & Zisserman, 2003; Özyeşil et al., 2017; Oliensis, 2000), which aims to estimate 3D geometry from a set of images. As a bridge between 2D images and the 3D world, it finds broad applications in diverse fields including autonomous driving (Huang et al., 2023; 2024), AR/VR (Zheng et al., 2024; Hong et al., 2024), and embodied robots (Wu et al., 2024; Wang et al., 2024b). With the development of embodied intelligence, on-the-fly 3D reconstruction from streaming inputs is increasingly demanded to enable online interactive visual systems, where latency and temporal consistency are crucial.

Conventional methods like Structurefrom-Motion (SfM) (Snavely et al., 2006; Agarwal et al., 2011; Frahm et al., 2010; Wu, 2013; Schönberger & Frahm, 2016; Liu et al., 2025) and Multi-View Stereo (MVS) (Furukawa & Ponce, 2009; Gu et al., 2020) rely on explicit geometric constraints (Furukawa et al., 2015; Galliani et al., 2015) or global optimization (Niemeyer et al., 2020; Fu et al., 2022; Wei et al., 2021; Yariv et al., 2020), limiting scalability and speed. Recent learningbased approaches have shifted toward endto-end frameworks that directly predict 3D structure from multi-view images. While pair-wise methods (Wang et al., 2024a; Leroy et al., 2024) have shown promising results by learning dense correspondences

054

055

057

058

060

061

062

063

064

065

066

067

068

069

070

071

072

073

074

075

076

077

079

081

082

083

084

085

086

087

880

089

090

091

092

094

096

098

099 100

101

102

103

104

105

106

107

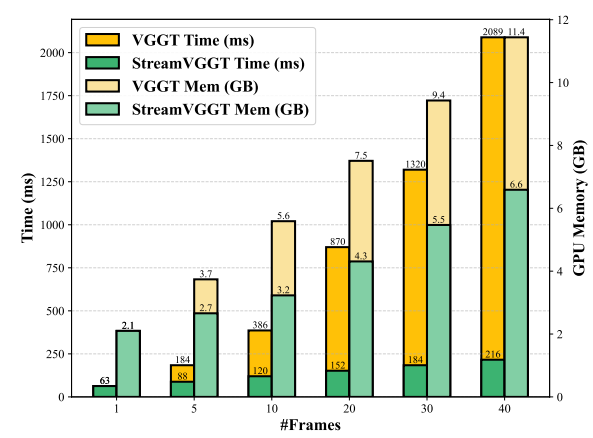


Figure 2: **Inference time and memory comparison** for the current frame of varying sequence lengths between StreamVGGT and VGGT for the online setting.

between image pairs, they utilize time-consuming post-processing steps for global alignment during multi-view reconstruction. Memory-augmented methods (Wang & Agapito, 2024; Wang et al., 2025b; Wu et al., 2025) maintain a memory pool to eliminate the need for post-processing. Additionally, their recursive memory update designs have the ability to address 3D reconstruction from videos. Nevertheless, error accumulation caused by causal architectures remains to be tackled. Fast3R (Yang et al., 2025) and VGGT (Wang et al., 2025a) circumvent iterative alignment by employing transformer-based feed-forward architectures that enable global dense-view interactions. Despite achieving satisfactory performance, their dependence on global self-attention necessitates reprocessing the entire sequence at every step for frame-by-frame input and output scenarios. This offline paradigm precludes incremental reconstruction and diverges from the causal nature of human perception, limiting its practicality in streaming applications.

In this paper, we propose StreamVGGT, a causal transformer architecture specifically designed for efficient, low-latency streaming 3D visual geometry reconstruction, as shown in Figure 1. Unlike conventional offline frameworks that necessitate reprocessing the entire sequence with the arrival of each new frame, we introduce a temporal causal attention mechanism combined with an implicit historical-token memory module. This allows incremental processing of video frames, enabling progressive scene updates in an online streaming manner. StreamVGGT leverages the inherent sequential and causal nature of real-world video data, constraining the attention mechanism to past and current frames, thereby aligning with the causal structure observed in human perception. Furthermore, to address the common challenge of long-term error accumulation inherent in causal models, we introduce a distillation-based training strategy. This strategy utilizes knowledge distillation from the densely connected, bidirectional visual geometry grounded transformer (VGGT) (Wang et al., 2025a) as the teacher model. By leveraging the global contextual understanding of the teacher model, our causal student model achieves stability and accuracy comparable to full-sequence inference. Equipped with FlashAttention-2 (Dao, 2023), our model supports fast inference for the current frame compared to VGGT, as shown in Figure 2. Experimental results demonstrate that our StreamVGGT significantly reduces inference overhead in long-term sequences with only a slight performance trade-off, representing a crucial step toward low-latency responsive 3D vision systems.

2 Related Work

Conventional 3D Reconstruction. 3D reconstruction, a fundamental task in computer vision (Hartley & Zisserman, 2000; Özyeşil et al., 2017; Oliensis, 2000), aims to recover the geometric structure of scenes from images or video sequences. Structure-from-Motion (SfM) (Snavely et al., 2006; Agarwal et al., 2011; Frahm et al., 2010; Wu, 2013; Schönberger & Frahm, 2016; Liu et al., 2025) reconstructs sparse 3D point clouds by matching image features across overlapping views and jointly refining camera poses and scene points through bundle adjustment (BA). A typical workflow comprises keypoint detection and description, feature matching with geometric verification, multi-view initialization and incremental camera registration, triangulation, and a global bundle adjustment. Although highly accurate in static scenes, SfM is fragile in dynamic or texture-poor environments

and, because of its computationally intensive offline optimization, cannot readily update in real time. Multi-View Stereo (MVS) (Furukawa et al., 2015; Galliani et al., 2015; Niemeyer et al., 2020; Fu et al., 2022; Wei et al., 2021; Yariv et al., 2020) exploits accurate camera poses to enforce photometric consistency across views, producing dense depth maps or point clouds that can be converted into high-resolution meshes or volumetric models. Neural Radiance Fields (NeRF) (Mildenhall et al., 2021) extend this idea by fitting the volume-rendering equation to learn a continuous radiance field, faithfully capturing fine-detail geometry and photometrically consistent appearance. Yet both MVS and NeRF depend on heavy offline optimisation, cannot update incrementally, and therefore provide limited low-latency capability. As a result, they are best employed as offline dense-reconstruction modules appended to an SfM pipeline rather than as online SLAM.

Learning-Based 3D Reconstruction. Building on the foundations of conventional 3D reconstruction, recent end-to-end, learning-based methods utilize neural networks to encode scene priors, markedly improving robustness and cross-dataset generalisation (Wang et al., 2024a; Leroy et al., 2024; Zhang et al., 2024; Smart et al., 2024; Fei et al., 2024; Dong et al., 2025). DUSt3R (Wang et al., 2024a) directly regresses view-consistent 3D point maps from just two RGB images without camera calibration, while its successor MASt3R (Leroy et al., 2024) introduces confidence-weighted losses to approximate metric scale. Recently, the feed-forward transformer-based architectures have emerged to enable dense-view interaction within a single pass (Yang et al., 2025; Wang et al., 2025a), delivering state-of-the-art accuracy in a few seconds. Fast3R (Yang et al., 2025) extends the pairwise DUSt3R idea to an N-view transformer equipped with memory-efficient Flash-Attention and parallel view fusion, allowing over 1000 images to be processed during inference. VGGT (Wang et al., 2025a) scales this philosophy to a 1.2B parameter visual geometry grounded transformer that jointly predicts camera intrinsics/extrinsics, dense depth, point maps, and 2D tracking features. However, its quadratic token-pair complexity and offline inference regime force complete re-encoding of every frame whenever a new image arrives. This heavy memory footprint and noncausal processing preclude streaming 3D reconstruction and undermine low-latency applications demanding instantaneous, frame-by-frame scene understanding.

Streaming 3D Reconstruction. low-latency streaming 3D reconstruction grows to be indispensable for autonomous driving, robotics, and AR/VR, where systems update scene geometry and camera pose on every frame with low latency (Wang & Agapito, 2024; Wang et al., 2025b; Wu et al., 2025). Spann3R (Wang & Agapito, 2024) augments a DUSt3R-style encoder with a token-addressable spatial memory, sustaining online point-map fusion but suffering drift on long or dynamic sequences due to its bounded memory. CUT3R (Wang et al., 2025b) introduces a recurrent transformer that jointly reads and writes a learnable scene state to output camera parameters, dense depth, and novelview completions in real time. However, it degrades when extrapolating far from observed regions, and demands heavy computation for recursive training. Point3R (Wu et al., 2025) couples an explicit geometry-aligned spatial pointer memory with 3D hierarchical RoPE and an adaptive fusion mechanism, delivering low-drift online pose, depth, and point-map updates in real time. Instead of designing the memory mechanism to store past information, we follow the philosophy of large language models and employ a causal transformer to implicitly cache historical visual tokens.

3 PROPOSED APPROACH

3.1 STREAMING 3D GEOMETRY RECONSTRUCTION

Given a set of images $\{I_t\}_{t=1}^T$, where each frame $I_t \in \mathbb{R}^{3 \times H \times W}$, the generic 3D reconstruction pipeline can be written as:

$$F_t = \operatorname{Encoder}(I_t), G_t = \operatorname{Decoder}(F_t), (P_t, C_t) = \operatorname{Head}(G_t),$$
 (1)

where the encoder maps each input frame I_t to a sequence of image tokens $F_t \in \mathbb{R}^{N \times C}$. A multiview decoder then fuses cross-frame information, producing geometry tokens $G_t \in \mathbb{R}^{N \times C}$, and a MLP head predicts a point map $P_t \in \mathbb{R}^{3 \times H \times W}$ together with a per-pixel confidence map $C_t \in \mathbb{R}^{H \times W}$ from these geometry tokens.

This formulation provides a unifying paradigm for 3D reconstruction, but state-of-the-art systems differ in how the decoder aggregates multi-view information, which can be grouped into three categories: pairwise, memory-augmented, and global interaction. Each framework introduced specialized modifications to the decoder and we summarize these designs as follows.

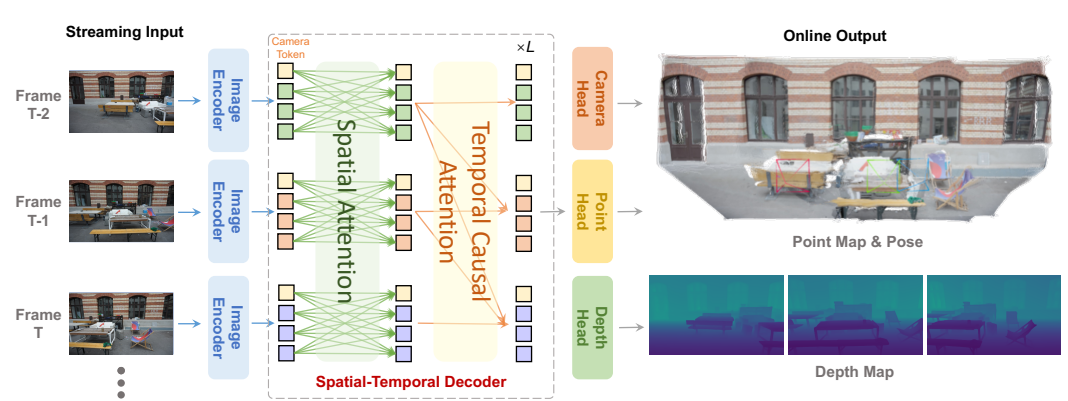


Figure 3: **Framework of StreamVGGT.** Our model consists of three main components: an image encoder, a spatio-temporal decoder, and multi-task prediction heads. During training, we utilize full-sequence inputs to provide the model with complete contextual information. To enforce temporal causality, we apply causal attention so the model can only attend to past frames at any given time step. This design encourages realistic temporal modeling suitable for streaming inference.

For pair-wise approaches like DUSt3R (Wang et al., 2024a) and MASt3R (Leroy et al., 2024), a two-branch cross-attention module jointly reasons over a reference/target pair, and no persistent state is kept beyond the current pair:

$$\{G_1, G_2\} = \text{Decoder}(\text{CrossAttn}(F_1, F_2)). \tag{2}$$

For memory-augmented approaches like Spann3R (Wang & Agapito, 2024) and CUT3R (Wang et al., 2025b), an external memory M_t updated online enables global consistency without post-processing during long sequence inference:

$$G_t, M_t = \text{Decoder}(\text{CrossAttn}(F_t, M_{t-1})).$$
 (3)

For global interaction approaches like Fast3R (Yang et al., 2025) and VGGT (Wang et al., 2025a), all frames attend to each other through all-to-all self-attention which achieves the highest accuracy at the cost of $\mathcal{O}(N^2)$ memory:

$$\{G_t\}_{t=1}^T = \text{Decoder}(\text{Global SelfAttn}(\{F_t\}_{t=1}^T)). \tag{4}$$

Although global interaction approaches have achieved impressive reconstruction accuracy, their reliance on global self-attention mechanisms inherently limits their ability to process streaming inputs efficiently. To overcome this limitation, we utilize a causal transformer architecture to explicitly model the causal structure intrinsic for streaming data. Specifically, for our StreamVGGT:

$$\{G_t\}_{t=1}^T = \text{Decoder}(\text{Temporal SelfAttn}(\{F_t\}_{t=1}^T)). \tag{5}$$

The temporal causal attention restricts each frame to attend only to itself and its predecessors, retaining rich context while reducing latency to $\mathcal{O}(N)$, which enables low-latency 3D perception.

3.2 Causal Architecture with Cached Memory Token

Building on the success of VGGT (Wang et al., 2025a), we propose a token-cached causal architecture consisting of three key components: image encoder, spatio-temporal decoder, and multi-task heads, as illustrated in Figure 3. We assume that the input images I are provided in sequential order, and all output attributes X are predicted frame by frame. This sequential input-output structure aligns with the causal perception logic observed in humans and is well-suited for low-latency 3D visual geometry reconstruction tasks, where spatial consistency and causality play a crucial role.

Image Encoder. We patchfy each input image I_t into a set of N image tokens $F_t \in \mathbb{R}^{N \times C}$ through DINO(Oquab et al., 2023). During the training stage, the image tokens of all frames are subsequently processed through our causal structure, alternating spatial and temporal attention layers.

Spatio-Temporal Decoder. We introduce the spatio-temporal decoder by replacing all the global self-attention layers with temporal attention layers. In the standard global self-attention mechanism,

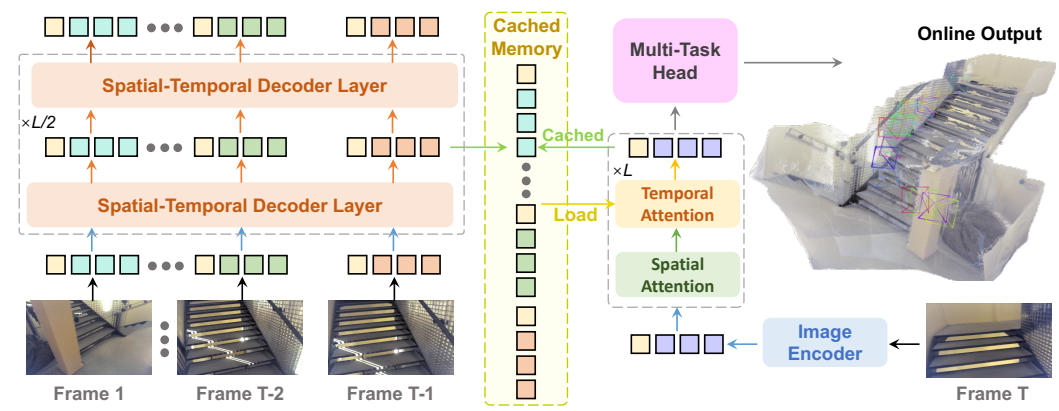


Figure 4: **Efficient inference of our model.** During streaming inference, we cache the historical keys and values as implicit memory to store information from past frames. This memory allows the model to efficiently reuse previously computed representations, avoiding redundant computation and enabling consistent contextual understanding across time. Our model then processes input incrementally and achieves performance that is comparable to full-sequence inference.

each image token F_t attends to all other tokens in the sequence, which can result in high computational costs when handling long sequences and is not well-suited for streaming 3D reconstruction tasks. In contrast, by using temporal attention, each token is restricted to attend only to the current and previous frames in the sequence, thereby respecting the inherent causal structure of the streaming inputs. This modification enables the model to maintain temporal consistency while significantly reducing the computational burden associated with global self-attention. In the training phase, we input all frames simultaneously, and the decoder generates geometry tokens G_t based solely on the context from the historical and current frames. This causal self-attention mechanism lays the foundation for enabling streaming input inference with minimal latency.

Cached Memory Token. Unlike the training phase, where all frames are input simultaneously and processed with temporal attention, streaming 3D reconstruction requires the model to handle frame-by-frame input and perform incremental 3D reconstruction during inference. To address this, we introduce an implicit memory mechanism that caches historical token $M \in \mathbb{R}^{T \times N \times C}$ from previously processed frames, as shown in Figure 4. During inference, StreamVGGT performs cross attention between the cached memory tokens and the image tokens derived from the current frame:

$$G_T = \text{Decoder}(\text{CrossAttn}(F_T, \{M_t\}_{t=1}^{T-1})), M_T = \text{TokenCachedMemory}(G_T).$$
 (6)

This design enables the model to replicate the temporal causal attention behavior observed during training. Through experimental validation, we demonstrate that the model with cached memory token achieves performance comparable to that of full-sequence input inference. This confirms the effectiveness of our approach in maintaining high performance during streaming 3D reconstruction, making it well-suited for low-latency visual geometry reconstruction tasks.

Multi-Task Heads. Following the VGGT architecture, we utilize three distinct task heads, each dedicated to predicting key 3D attributes X of the scene. These heads are responsible for estimating the camera pose $g_t \in \mathbb{R}^9$, point maps $P_t \in \mathbb{R}^{3 \times H \times W}$, depth maps $D_t \in \mathbb{R}^{H \times W}$, and point tracks $y_t \in \mathbb{R}^{2 \times M}$ from every single frame. Specifically, for each input image I_t , the image tokens F_t produced by the image encoder are subsequently fed into the decoder to generate the geometry tokens G_t . The geometry tokens are then passed through specialized task heads that predict the desired 3D attributes. We also leverage a learnable camera token to mark the first frame as the global reference, so all subsequent frames are incrementally aligned within this shared coordinate system, enabling consistent, streaming 3D reconstruction without post-processing.

Camera Head. This head is responsible for predicting the intrinsic and extrinsic camera parameters. The output consists of the translation vector, rotation quaternion, and field of view (FoV), which together describe the pose of the camera in 3D space. The Camera Head uses self-attention layers to refine the camera parameters for each input frame.

Geometry Head. This head generates both the point map and depth map for each frame. Additionally, it outputs confidence maps (Kendall & Cipolla, 2016; Novotny et al., 2018) for both the point

and depth predictions, indicating the certainty of the model in various regions. This head also produces dense tracking features, which are passed to the Track Head for point tracking across frames. Specifically, it leverages a DPT layer (Ranftl et al., 2021) to convert geometry tokens into dense feature maps, which are then processed by convolutional layers to produce the final point and depth maps with their corresponding confidence maps.

3.3 DISTILLATION-BASED TRAINING

Knowledge Distillation. We introduce a knowledge distillation strategy (KD), where a teacher model uses global attention to guide the causal student model. The teacher processes all frames in the sequence to captures richer context and outputs both a prediction and a per-pixel confidence map. We weight the regression loss by this confidence, so high-confidence regions back-propagate strong gradients while low-confidence regions contribute almost none. This selective focus lets the student learn from the most informative regions and also teaches the model to down-weight low-confidence past observations, where the student model is able to maintain high accuracy with higher efficiency.

Moreover, knowledge distillation helps achieve better performance at comparable training costs, allowing us to obtain a satisfactory model with fewer GPU hours. In addition, KD enhances the model's generalization ability (Furlanello et al., 2018; Romero et al., 2014). To further validate this, we present an ablation study on the effectiveness of knowledge distillation in Section 4.6.

Training Loss. We follow the loss design from VGGT (Wang et al., 2025a) but introduce a key difference: we use the output of a teacher model as pseudo-ground truth to supervise our causal student model. This strategy helps mitigate error accumulation, which arises in causal models that only have access to current and historical frames. The loss function is:

$$L = L_{\text{camera}} + L_{\text{depth}} + L_{\text{pmap}}.$$
 (7)

The camera loss L_{camera} supervises the predicted camera parameters \hat{g}_i by comparing them to the ground-truth camera parameters g_i . This is done using the Huber loss function:

$$L_{\text{camera}} = \sum_{i=1}^{N} \|\hat{g}_i - g_i\|_{\epsilon}, \tag{8}$$

where $\|\cdot\|_{\epsilon}$ represents the Huber loss function, which is robust to outliers in the data.

The depth loss L_{depth} incorporates depth confidence, which weighs the discrepancy between the predicted depth \hat{D}_i and the ground-truth depth D_i with the predicted confidence map $\hat{\Sigma}_i^D$. The gradient-based term is applied to further refine the depth estimation, which is commonly used in monocular depth estimation tasks. The final form of the depth loss is:

$$L_{\text{depth}} = \sum_{i=1}^{N} \|\hat{\Sigma}_{i}^{D} \odot (\hat{D}_{i} - D_{i})\| + \|\hat{\Sigma}_{i}^{D} \odot (\nabla \hat{D}_{i} - \nabla D_{i})\| - \alpha \log \hat{\Sigma}_{i}^{D}, \tag{9}$$

where \odot denotes the element-wise product, and ∇ represents the gradient.

The point map loss L_{pmap} is defined similarly to the depth loss but for the 3D point map. It takes into account the point-map confidence Σ_i^P and ensures that the predicted 3D points \hat{P}_i match the ground-truth points P_i . The loss is formulated as:

$$L_{\text{pmap}} = \sum_{i=1}^{N} \|\Sigma_{i}^{P} \odot (\hat{P}_{i} - P_{i})\| + \|\Sigma_{i}^{P} \odot (\nabla \hat{P}_{i} - \nabla P_{i})\| - \alpha \log \Sigma_{i}^{P}.$$
 (10)

Our framework unifies batch training and frame-by-frame inference through a causal, memory-cached architecture. During training, the student model leverages teacher guidance via knowledge distillation, enabling it to learn effective spatio-temporal representations while maintaining training efficiency. During inference, the cached memory tokens allow the model to process streaming inputs incrementally, replicating the causal behavior observed during training without sacrificing accuracy. This design ensures both high training efficiency and low-latency inference, making our method particularly well-suited for streaming 3D reconstruction.

Table 1: Quantitative 3D reconstruction results on 7-Scenes and NRGBD datasets.

		7 scenes							NRGBD					
		Ac	Acc↓		Comp↓		NC↑		Acc↓		Comp↓		C↑	
Method	Type	Mean	Med.	Mean	Med.	Mean	Med.	Mean	Med.	Mean	Med.	Mean	Med.	
DUSt3R-GA (Wang et al., 2024a)	Pair-wise	0.146	0.077	0.181	0.067	0.736	0.839	0.144	0.019	0.154	0.018	0.870	0.982	
MASt3R-GA (Leroy et al., 2024)	Pair-wise	0.185	0.081	0.180	0.069	0.701	0.792	0.085	0.033	0.063	0.028	0.794	0.928	
MonST3R-GA (Zhang et al., 2024)	Pair-wise	0.248	0.185	0.266	0.167	0.672	0.759	0.272	0.114	0.287	0.110	0.758	0.843	
VGGT (Wang et al., 2025a)	Dense-view	0.088	0.039	0.091	0.039	0.787	0.890	0.073	0.018	0.077	0.021	0.910	0.990	
Spann3R (Wang & Agapito, 2024)	Streaming	0.298	0.226	0.205	0.112	0.650	0.730	0.416	0.323	0.417	0.285	0.684	0.789	
CUT3R (Wang et al., 2025b)	Streaming	0.126	0.047	0.154	0.031	0.727	0.834	0.099	0.031	0.076	0.026	0.837	0.971	
StreamVGGT	Streaming	0.129	0.056	0.115	0.041	0.751	0.865	0.084	0.044	0.074	0.041	0.861	0.986	

Table 2: Quantitative 3D reconstruction results on ETH3D dataset.

Methods	Type	Acc.↓	Comp.↓	Overall↓
DUSt3R (Wang et al., 2024a)	Pair-wise	1.167	0.842	1.005
MASt3R (Leroy et al., 2024)	Pair-wise	0.968	0.684	0.826
VGGT (Wang et al., 2025a)	Dense-view	0.928	0.443	0.686
CUT3R (Wang et al., 2025b)	Streaming	1.426	1.395	1.411
StreamVGGT	Streaming	0.609	0.545	0.577

4 EXPERIMENTS

4.1 IMPLEMENTATION DETAILS

Our model architecture follows VGGT (Wang et al., 2025a) with L = 24 layers of temporal and spatial attention modules. We integrated FlashAttention-2 (Dao, 2023) to accelerate the inference. We initialized StreamVGGT by using pre-trained weights from VGGT and fine-tuned approximately 950 million parameters (excluding the frozen image backbone) for 10 epochs. We employed the AdamW optimizer and a hybrid schedule of linear warm-up (first 0.5 epochs) followed by cosine decay, reaching a peak learning rate of 1e-6. For each training iteration, we randomly sampled a batch of 10 frames from diverse training scenes. Following Point3R (Wu et al., 2025), we processed input images with variable aspect ratios while resizing the maximum edge length to 518 pixels. Training was conducted on 4 NVIDIA A800 GPUs for 7 days.

4.2 Training Datasets

Our StreamVGGT was fine-tuned on a curated multi-domain collection comprising 13 datasets: Co3Dv2 (Reizenstein et al., 2021), BlendMVS (Yao et al., 2020), ARKitScenes (Baruch et al., 2021), MegaDepth (Li & Snavely, 2018), WildRGB (Xia et al., 2024), ScanNet (Dai et al., 2017), HyperSim (Roberts et al., 2021), OmniObject3D (Wu et al., 2023), MVS-Synth (Huang et al., 2018), PointOdyssey (Zheng et al., 2023), Virtual KITTI (Cabon et al., 2020), Spring (Mehl et al., 2023), and Waymo (Sun et al., 2020). This collection covers diverse visual domains spanning indoor/outdoor environments and temporal scales and balances synthetic data and real-world captures.

4.3 3D RECONSTRUCTION

Comparisons on the 7-scenes and NRGBD datasets. Following CUT3R (Wang et al., 2025b), we evaulated the 3D reconstruction performance of StreamVGGT on 7-Scenes (Shotton et al., 2013) and NRGBD (Azinović et al., 2022). Accuracy (Acc), completeness (Comp), and normal-consistency (NC) scores are reported using sparse inputs (3–5 frames per scene on 7-Scenes and 2–4 frames per scene on NRGBD). Table 1 show that StreamVGGT performs competitively against existing streaming methods and surpasses the state-of-the-art streaming model CUT3R (Wang et al., 2025b).

Comparisons on the ETH3D dataset. Following VGGT (Wang et al., 2025a), we further evaluated the accuracy of the predicted point clouds on the ETH3D (Schops et al., 2017) dataset. For each scene, we randomly sampled 10 frames and report the results after discarding invalid points using the official valid masks. Specifically, we measure accuracy (Acc), completeness (Comp), and overall quality (Chamfer distance) for 3D reconstruction. Table 2 shows that StreamVGGT surpasses DUSt3R and MASt3R and matches the performance of the current state-of-the-art VGGT, despite relying solely on information from the current and past frames. Note that our causal design enables streaming 3D reconstruction and is more efficient than VGGT.

378 379

380

386 387 388

397

399 400 401

402

403

404

409

410

411

412 413 414

415 416

417

427

428

429

430

431

422

Table 3: Single-Frame Depth Evaluation.

	<u> </u>												
		Sintel		Во	onn	KI	TTI	NYU-v2	2 (Static)				
Method	Type	Abs Rel↓	$\delta < 1.25 \uparrow$	Abs Rel↓	$\delta < 1.25 \uparrow$	Abs Rel ↓	$\delta < 1.25 \uparrow$	Abs Rel↓	$\delta < 1.25 \uparrow$				
DUSt3R (Wang et al., 2024a) MASt3R (Leroy et al., 2024) MonST3R (Zhang et al., 2024) VGGT (Wang et al., 2025a)	Pair-wise Pair-wise Pair-wise Dense-view	0.424 <u>0.340</u> 0.358 0.276	58.7 <u>60.4</u> 54.8 67.5	0.141 0.142 <u>0.076</u> 0.055	82.5 82.0 93.9 97.1	0.112 0.079 0.100 0.072	86.3 94.7 89.3 <u>93.8</u>	0.080 0.129 0.102 0.060	90.7 84.9 88.0 95.1				
Spann3R (Wang & Agapito, 2024) CUT3R (Wang et al., 2025b) Point3R (Wu et al., 2025) StreamVGGT	Streaming Streaming Streaming Streaming	0.470 0.428 <u>0.395</u> 0.254	53.9 55.4 <u>56.8</u> 68.5	0.118 0.063 <u>0.061</u> 0.052	85.9 <u>96.2</u> <u>95.4</u> 97.1	0.128 0.092 0.087 0.072	84.6 91.3 <u>93.7</u> 94.7	0.122 0.086 0.079 0.055	84.9 90.9 92.0 95.9				

Table 4: Video Depth Evaluation.

		Sin	ntel	ВО	NN	KIT	TI
Method	Type	Abs Rel↓	$\delta < 1.25 \uparrow$	Abs Rel↓	$\delta < 1.25 \uparrow$	Abs Rel↓	$\delta < 1.25 \uparrow$
DUSt3R-GA (Wang et al., 2024a)	Pair-wise	0.656	45.2	0.155	83.3	0.144	81.3
MASt3R-GA (Leroy et al., 2024)	Pair-wise	0.641	43.9	0.252	70.1	0.183	74.5
MonST3R-GA (Zhang et al., 2024)	Pair-wise	<u>0.378</u>	55.8	<u>0.067</u>	96.3	0.168	74.4
VGGT (Wang et al., 2025a)	Dense-view	0.298	68.1	0.057	96.8	0.061	97.0
Spann3R (Wang & Agapito, 2024)	Streaming	0.622	42.6	0.144	81.3	0.198	73.7
CUT3R (Wang et al., 2025b)	Streaming	<u>0.421</u>	47.9	0.078	93.7	0.118	88.1
Point3R (Wu et al., 2025)	Streaming	<u>0.452</u>	48.9	<u>0.060</u>	<u>96.0</u>	<u>0.136</u>	84.2
StreamVGGT	Streaming	0.323	65.7	0.059	97.2	0.173	72.1

4.4 SINGLE-FRAME AND VIDEO DEPTH ESTIMATION

Single-Frame Depth Estimation. Following MonST3R (Zhang et al., 2024), we evaluated singleframe depth estimation across four datasets: KITTI (Geiger et al., 2013), Sintel (Alnegheimish et al., 2022), Bonn (Palazzolo et al., 2019), and NYU-v2 (Silberman et al., 2012), encompassing both dynamic/static scenes and indoor/outdoor environments. To ensure unbiased evaluation of cross-domain generalization, these datasets were strictly excluded during training. Following DUSt3R (Wang et al., 2024a), we employ two principal metrics: Absolute Relative Error (Abs Rel) and the percentage of predictions within a 1.25 factor of ground truth depth (δ 1.25). Table 3 shows that our method not only matches the overall best performers but also outperforms the current stateof-the-art streaming model on all datasets, showing its superiority for online depth estimation.

Video Depth Estimation. We conducted video depth estimation by assessing both the depth quality on a per-frame basis and the consistency of depth across frames. This was done by aligning the predicted depth maps with the ground truth using a per-sequence scale. We show the comparison of these methods in Table 4. Under aligned settings, our StreamVGGT exceeds CUT3R on both the Sintel and Bonn benchmarks and attains performance comparable to the offline VGGT.

4.5 CAMERA POSE ESTIMATION

Table 5 shows the camera-pose estimation results on ScanNet (Dai et al., 2017), Sintel (Alnegheimish et al., 2022) and TUM dynamics (Sturm et al., 2012). Both Sintel and TUM-dynamics contain dynamic objects, which pose substantial challenges for conventional Structure-from-Motion (SfM) and SLAM methods. We evaluate performance by reporting the Absolute Translation Error (ATE), Relative Translation Error (RPE trans), and Relative Rotation Error (RPE rot), all computed after applying Sim(3) alignment with the ground truth trajectories. StreamVGGT delivers performance on par with the best existing methods while uniquely supporting camera-pose prediction from streaming inputs, highlighting its practicality for low-latency applications.

4.6 EXPERIMENTAL ANALYSIS

Inference Time and Memory Consumption Analysis. To evaluate the efficiency of our design in streaming tasks, we compare the inference latency for the final frame of sequences containing 1, 5, 10, 20, 30, and 40 frames among StreamVGGT and VGGT (Wang et al., 2025a). All experiments were conducted on a single NVIDIA A800 GPU. For StreamVGGT and VGGT, we employ FlashAttention-2 (Dao, 2023) with an image resolution of 518×392 . The results of inference time and memory consumption are summarized in Figure 2.

Table 5: Camera Pose Estimation Evaluation on ScanNet, Sintel, and TUM-dynamics datasets.

		ScanNet			Sintel			TUM-dynamics		
Method	Type	ATE↓	RPE trans	↓ RPE rot ↓	, ATE↓	RPE trans	RPE rot	.∤ATE↓	RPE trans .	↓ RPE rot ↓
Robust-CVD (Kopf et al., 2021)	Pair-wise	0.227	0.064	7.374	0.360	0.154	3.443	0.153	0.026	3.528
CasualSAM (Zhang et al., 2022)	Pair-wise	0.158	0.034	1.618	0.141	0.035	0.615	0.071	0.010	1.712
DUSt3R-GA (Wang et al., 2024a)	Pair-wise	0.081	0.028	0.784	0.417	0.250	5.796	0.083	0.017	3.567
MASt3R-GA (Leroy et al., 2024)	Pair-wise	0.078	0.020	0.475	0.185	0.060	1.496	0.038	0.012	0.448
MonST3R-GA (Zhang et al., 2024)	Pair-wise	0.077	0.018	0.529	0.111	0.044	0.869	0.098	0.019	0.935
VGGT (Wang et al., 2025a)	Dense-view	0.035	0.015	0.377	0.169	0.064	0.474	0.012	0.010	0.307
Spann3R (Wang & Agapito, 2024)	Streaming	0.096	0.023	0.661	0.329	0.110	4.471	0.056	0.021	0.591
CUT3R (Wang et al., 2025b)	Streaming	0.099	0.022	0.600	0.213	0.066	0.621	0.046	0.015	0.473
Point3R (Wu et al., 2025)	Streaming	0.106	0.035	1.946	0.351	0.128	1.822	0.075	0.029	0.642
StreamVGGT	Streaming	0.048	0.019	0.557	0.219	0.103	1.041	0.026	0.012	0.316

Table 6: Effects of the distillation training strategy.

		·	·			7 sc	enes					NRO	GBD		
				Ac	:c↓	Cor	np↓	N	 C↑	Ac	Acc↓ Comp↓		np↓	N	 C↑
1	Method	Distillation	Attention	Mean	Med.	Mean	Med.	Mean	Med.	Mean	Med.	Mean	Med.	Mean	Med.
StreamV	Vang et al., 2025a) VGGT (w/o KD) VGGT (W/ KD)	✓	Global Causal Causal	0.202	0.102	0.168	0.064	0.718	0.825	0.189	0.088	0.077 0.206 0.074	0.096	0.816	0.945
CUT3R															Y
Ours					4										
GT	THE LANGE THE PARTY OF THE PART											2/1	Y.		

Figure 5: Qualitative comparisons with CUT3R (Wang et al., 2025b).

Distillation Training Strategy. To assess the effectiveness of our knowledge-distillation strategy, we evaluated three variants on the 7-Scenes, NRGBD, and ETH3D datasets: (i) the global self-attention teacher VGGT, (ii) StreamVGGT without knowledge distillation, and (iii) StreamVGGT with knowledge distillation. Table 6 demonstrates that the causal model without distillation shows significantly higher reconstruction errors, demonstrating its limited frame context. After distillation, the performance gap between StreamVGGT and VGGT across all 3D reconstruction metrics remains within an acceptable range, while the model still benefits from a low-latency, streaming design.

Visualizations. StreamVGGT delivers photorealistic scene reconstructions with superior geometric fidelity, fewer outliers, and accuracy in complex environments, as shown in Figure 7.

More Experiments. We provide more experimental results in Appendix A.1 and Appendix A.2.

5 CONCLUSION

In this paper, we have presented StreamVGGT, a causal transformer architecture for low-latency streaming 3D visual geometry reconstruction. By replacing global self-attention with causal temporal attention and introducing a cached token memory mechanism, StreamVGGT achieves incremental scene updates while preserving long-term spatial consistency. Extensive experiments demonstrate that StreamVGGT achieves comparable accuracy to the state-of-the-art offline model VGGT with small performance degradation, while surpassing current online state-of-the-art models across multiple tasks, including 3D reconstruction, single-frame depth estimation, and depth estimation.

REFERENCES

- Sameer Agarwal, Yasutaka Furukawa, Noah Snavely, Ian Simon, Brian Curless, Steven M Seitz, and Richard Szeliski. Building rome in a day. *Communications of the ACM*, 54(10):105–112, 2011.
- Sarah Alnegheimish, Dongyu Liu, Carles Sala, Laure Berti-Equille, and Kalyan Veeramachaneni. Sintel: A machine learning framework to extract insights from signals. In *SIGMOD*, pp. 1855–1865, 2022.
 - Dejan Azinović, Ricardo Martin-Brualla, Dan B Goldman, Matthias Nießner, and Justus Thies. Neural rgb-d surface reconstruction. In *CVPR*, pp. 6290–6301, 2022.
 - Gilad Baruch, Zhuoyuan Chen, Afshin Dehghan, Tal Dimry, Yuri Feigin, Peter Fu, Thomas Gebauer, Brandon Joffe, Daniel Kurz, Arik Schwartz, et al. Arkitscenes: A diverse real-world dataset for 3d indoor scene understanding using mobile rgb-d data. *arXiv preprint arXiv:2111.08897*, 2021.
 - Yohann Cabon, Naila Murray, and Martin Humenberger. Virtual kitti 2. *arXiv preprint arXiv:2001.10773*, 2020.
 - Angela Dai, Angel X Chang, Manolis Savva, Maciej Halber, Thomas Funkhouser, and Matthias Nießner. Scannet: Richly-annotated 3d reconstructions of indoor scenes. In *CVPR*, pp. 5828–5839, 2017.
 - Tri Dao. Flashattention-2: Faster attention with better parallelism and work partitioning. *arXiv* preprint arXiv:2307.08691, 2023.
 - Siyan Dong, Shuzhe Wang, Shaohui Liu, Lulu Cai, Qingnan Fan, Juho Kannala, and Yanchao Yang. Reloc3r: Large-scale training of relative camera pose regression for generalizable, fast, and accurate visual localization. In *CVPR*, pp. 16739–16752, 2025.
 - Xin Fei, Wenzhao Zheng, Yueqi Duan, Wei Zhan, Masayoshi Tomizuka, Kurt Keutzer, and Jiwen Lu. Driv3r: Learning dense 4d reconstruction for autonomous driving. *arXiv preprint arXiv:2412.06777*, 2024.
 - Jan-Michael Frahm, Pierre Fite-Georgel, David Gallup, Tim Johnson, Rahul Raguram, Changchang Wu, Yi-Hung Jen, Enrique Dunn, Brian Clipp, Svetlana Lazebnik, et al. Building rome on a cloudless day. In *ECCV*, pp. 368–381. Springer, 2010.
 - Qiancheng Fu, Qingshan Xu, Yew Soon Ong, and Wenbing Tao. Geo-neus: Geometry-consistent neural implicit surfaces learning for multi-view reconstruction. *NeurIPS*, 35:3403–3416, 2022.
 - Tommaso Furlanello, Zachary Lipton, Michael Tschannen, Laurent Itti, and Anima Anandkumar. Born again neural networks. In *ICML*, pp. 1607–1616, 2018.
 - Yasutaka Furukawa and Jean Ponce. Accurate, dense, and robust multiview stereopsis. *TPAMI*, 32 (8):1362–1376, 2009.
 - Yasutaka Furukawa, Carlos Hernández, et al. Multi-view stereo: A tutorial. *Foundations and Trends® in Computer Graphics and Vision*, 9(1-2):1–148, 2015.
 - Silvano Galliani, Katrin Lasinger, and Konrad Schindler. Massively parallel multiview stereopsis by surface normal diffusion. In *ICCV*, pp. 873–881, 2015.
- Andreas Geiger, Philip Lenz, Christoph Stiller, and Raquel Urtasun. Vision meets robotics: The kitti dataset. *IJRR*, 32(11):1231–1237, 2013.
- Xiaodong Gu, Zhiwen Fan, Siyu Zhu, Zuozhuo Dai, Feitong Tan, and Ping Tan. Cascade cost volume for high-resolution multi-view stereo and stereo matching. In *CVPR*, pp. 2495–2504, 2020.
- Richard Hartley and Andrew Zisserman. *Multiple View Geometry in Computer Vision*. Cambridge University Press, 2000.
 - Richard Hartley and Andrew Zisserman. *Multiple view geometry in computer vision*. Cambridge university press, 2003.

- Jin Gyu Hong, Seung Young Noh, Hee Kyung Lee, Won Sik Cheong, and Ju Yong Chang. 3d clothed human reconstruction from sparse multi-view images. In *CVPR*, pp. 677–687, 2024.
- Nan Huang, Xiaobao Wei, Wenzhao Zheng, Pengju An, Ming Lu, Wei Zhan, Masayoshi Tomizuka, Kurt Keutzer, and Shanghang Zhang. Sgaussian: Self-supervised street gaussians for autonomous driving. *CoRR*, 2024.
 - Po-Han Huang, Kevin Matzen, Johannes Kopf, Narendra Ahuja, and Jia-Bin Huang. Deepmvs: Learning multi-view stereopsis. In *CVPR*, 2018.
 - Yuanhui Huang, Wenzhao Zheng, Yunpeng Zhang, Jie Zhou, and Jiwen Lu. Tri-perspective view for vision-based 3d semantic occupancy prediction. In *CVPR*, pp. 9223–9232, 2023.
 - Alex Kendall and Roberto Cipolla. Modelling uncertainty in deep learning for camera relocalization. In *ICRA*, pp. 4762–4769. IEEE, 2016.
 - Johannes Kopf, Xuejian Rong, and Jia-Bin Huang. Robust consistent video depth estimation. In *CVPR*, pp. 1611–1621, 2021.
 - Vincent Leroy, Yohann Cabon, and Jérôme Revaud. Grounding image matching in 3d with mast3r. *arXiv preprint arXiv:2406.09756*, 2024.
 - Zhengqi Li and Noah Snavely. Megadepth: Learning single-view depth prediction from internet photos. In *CVPR*, pp. 2041–2050, 2018.
- Shaohui Liu, Yidan Gao, Tianyi Zhang, Rémi Pautrat, Johannes L Schönberger, Viktor Larsson, and Marc Pollefeys. Robust incremental structure-from-motion with hybrid features. In *ECCV*, pp. 249–269. Springer, 2025.
 - Lukas Mehl, Jenny Schmalfuss, Azin Jahedi, Yaroslava Nalivayko, and Andrés Bruhn. Spring: A high-resolution high-detail dataset and benchmark for scene flow, optical flow and stereo. In *CVPR*, pp. 4981–4991, 2023.
 - Ben Mildenhall, Pratul P Srinivasan, Matthew Tancik, Jonathan T Barron, Ravi Ramamoorthi, and Ren Ng. Nerf: Representing scenes as neural radiance fields for view synthesis. *Communications of the ACM*, 65(1):99–106, 2021.
 - Michael Niemeyer, Lars Mescheder, Michael Oechsle, and Andreas Geiger. Differentiable volumetric rendering: Learning implicit 3d representations without 3d supervision. In *CVPR*, pp. 3504–3515, 2020.
 - David Novotny, Diane Larlus, and Andrea Vedaldi. Capturing the geometry of object categories from video supervision. *TPAMI*, 42(2):261–275, 2018.
 - John Oliensis. A critique of structure-from-motion algorithms. CVIU, 80(2):172–214, 2000.
 - Maxime Oquab, Timothée Darcet, Théo Moutakanni, Huy Vo, Marc Szafraniec, Vasil Khalidov, Pierre Fernandez, Daniel Haziza, Francisco Massa, Alaaeldin El-Nouby, et al. Dinov2: Learning robust visual features without supervision. *arXiv preprint arXiv:2304.07193*, 2023.
 - Onur Özyeşil, Vladislav Voroninski, Ronen Basri, and Amit Singer. A survey of structure from motion*. *Acta Numerica*, 26:305–364, 2017.
- Emanuele Palazzolo, Jens Behley, Philipp Lottes, Philippe Giguere, and Cyrill Stachniss. Refusion: 3d reconstruction in dynamic environments for rgb-d cameras exploiting residuals. In *IROS*, pp. 7855–7862. IEEE, 2019.
 - René Ranftl, Alexey Bochkovskiy, and Vladlen Koltun. Vision transformers for dense prediction. In *ICCV*, pp. 12179–12188, 2021.
 - Jeremy Reizenstein, Roman Shapovalov, Philipp Henzler, Luca Sbordone, Patrick Labatut, and David Novotny. Common objects in 3d: Large-scale learning and evaluation of real-life 3d category reconstruction. In *ICCV*, pp. 10901–10911, 2021.

- Mike Roberts, Jason Ramapuram, Anurag Ranjan, Atulit Kumar, Miguel Angel Bautista, Nathan Paczan, Russ Webb, and Joshua M Susskind. Hypersim: A photorealistic synthetic dataset for holistic indoor scene understanding. In *ICCV*, pp. 10912–10922, 2021.
 - Adriana Romero, Nicolas Ballas, Samira Ebrahimi Kahou, Antoine Chassang, Carlo Gatta, and Yoshua Bengio. Fitnets: Hints for thin deep nets. arxiv 2014. *arXiv preprint arXiv:1412.6550*, 2014.
 - Johannes Lutz Schönberger and Jan-Michael Frahm. Structure-from-motion revisited. In *CVPR*, 2016.
 - Thomas Schops, Johannes L Schonberger, Silvano Galliani, Torsten Sattler, Konrad Schindler, Marc Pollefeys, and Andreas Geiger. A multi-view stereo benchmark with high-resolution images and multi-camera videos. In *CVPR*, pp. 3260–3269, 2017.
 - Jamie Shotton, Ben Glocker, Christopher Zach, Shahram Izadi, Antonio Criminisi, and Andrew Fitzgibbon. Scene coordinate regression forests for camera relocalization in rgb-d images. In CVPR, pp. 2930–2937, 2013.
 - Nathan Silberman, Derek Hoiem, Pushmeet Kohli, and Rob Fergus. Indoor segmentation and support inference from rgbd images. In *ECCV*, pp. 746–760. Springer, 2012.
 - Brandon Smart, Chuanxia Zheng, Iro Laina, and Victor Adrian Prisacariu. Splatt3r: Zero-shot gaussian splatting from uncalibrated image pairs. *arXiv preprint arXiv:2408.13912*, 2024.
 - Noah Snavely, Steven M Seitz, and Richard Szeliski. Photo tourism: exploring photo collections in 3d. In *SIGGRAPH*, pp. 835–846. 2006.
 - Jürgen Sturm, Nikolas Engelhard, Felix Endres, Wolfram Burgard, and Daniel Cremers. A benchmark for the evaluation of rgb-d slam systems. In *IROS*, pp. 573–580. IEEE, 2012.
 - Pei Sun, Henrik Kretzschmar, Xerxes Dotiwalla, Aurelien Chouard, Vijaysai Patnaik, Paul Tsui, James Guo, Yin Zhou, Yuning Chai, Benjamin Caine, et al. Scalability in perception for autonomous driving: Waymo open dataset. In *CVPR*, pp. 2446–2454, 2020.
 - Hengyi Wang and Lourdes Agapito. 3d reconstruction with spatial memory. arXiv preprint arXiv:2408.16061, 2024.
 - Jianyuan Wang, Minghao Chen, Nikita Karaev, Andrea Vedaldi, Christian Rupprecht, and David Novotny. Vggt: Visual geometry grounded transformer. In *CVPR*, pp. 5294–5306, 2025a.
 - Qianqian Wang, Yifei Zhang, Aleksander Holynski, Alexei A. Efros, and Angjoo Kanazawa. Continuous 3d perception model with persistent state, 2025b.
 - Shuzhe Wang, Vincent Leroy, Yohann Cabon, Boris Chidlovskii, and Jerome Revaud. Dust3r: Geometric 3d vision made easy. In *CVPR*, pp. 20697–20709, 2024a.
 - Tai Wang, Xiaohan Mao, Chenming Zhu, Runsen Xu, Ruiyuan Lyu, Peisen Li, Xiao Chen, Wenwei Zhang, Kai Chen, Tianfan Xue, et al. Embodiedscan: A holistic multi-modal 3d perception suite towards embodied ai. In *CVPR*, pp. 19757–19767, 2024b.
 - Yi Wei, Shaohui Liu, Yongming Rao, Wang Zhao, Jiwen Lu, and Jie Zhou. Nerfingmvs: Guided optimization of neural radiance fields for indoor multi-view stereo. In *ICCV*, pp. 5610–5619, October 2021.
- Changchang Wu. Towards linear-time incremental structure from motion. In *3DV*, pp. 127–134. IEEE, 2013.
 - Tong Wu, Jiarui Zhang, Xiao Fu, Yuxin Wang, Jiawei Ren, Liang Pan, Wayne Wu, Lei Yang, Jiaqi Wang, Chen Qian, et al. Omniobject3d: Large-vocabulary 3d object dataset for realistic perception, reconstruction and generation. In *CVPR*, pp. 803–814, 2023.
 - Yuqi Wu, Wenzhao Zheng, Sicheng Zuo, Yuanhui Huang, Jie Zhou, and Jiwen Lu. Embodiedocc: Embodied 3d occupancy prediction for vision-based online scene understanding. *arXiv* preprint *arXiv*:2412.04380, 2024.

- Yuqi Wu, Wenzhao Zheng, Jie Zhou, and Jiwen Lu. Point3r: Streaming 3d reconstruction with explicit spatial pointer memory. In *NeurIPS*, 2025.
- Hongchi Xia, Yang Fu, Sifei Liu, and Xiaolong Wang. Rgbd objects in the wild: scaling real-world 3d object learning from rgb-d videos. In *CVPR*, pp. 22378–22389, 2024.
- Jianing Yang, Alexander Sax, Kevin J Liang, Mikael Henaff, Hao Tang, Ang Cao, Joyce Chai, Franziska Meier, and Matt Feiszli. Fast3r: Towards 3d reconstruction of 1000+ images in one forward pass. *arXiv preprint arXiv:2501.13928*, 2025.
- Yao Yao, Zixin Luo, Shiwei Li, Jingyang Zhang, Yufan Ren, Lei Zhou, Tian Fang, and Long Quan. Blendedmys: A large-scale dataset for generalized multi-view stereo networks. In *CVPR*, pp. 1790–1799, 2020.
- Lior Yariv, Yoni Kasten, Dror Moran, Meirav Galun, Matan Atzmon, Basri Ronen, and Yaron Lipman. Multiview neural surface reconstruction by disentangling geometry and appearance. *NeurIPS*, 33:2492–2502, 2020.
- Junyi Zhang, Charles Herrmann, Junhwa Hur, Varun Jampani, Trevor Darrell, Forrester Cole, Deqing Sun, and Ming-Hsuan Yang. Monst3r: A simple approach for estimating geometry in the presence of motion. *arXiv preprint arXiv:2410.03825*, 2024.
- Zhoutong Zhang, Forrester Cole, Zhengqi Li, Michael Rubinstein, Noah Snavely, and William T Freeman. Structure and motion from casual videos. In *ECCV*, pp. 20–37. Springer, 2022.
- Shunyuan Zheng, Boyao Zhou, Ruizhi Shao, Boning Liu, Shengping Zhang, Liqiang Nie, and Yebin Liu. Gps-gaussian: Generalizable pixel-wise 3d gaussian splatting for real-time human novel view synthesis. In *CVPR*, pp. 19680–19690, 2024.
- Yang Zheng, Adam W. Harley, Bokui Shen, Gordon Wetzstein, and Leonidas J. Guibas. Pointodyssey: A large-scale synthetic dataset for long-term point tracking. In *ICCV*, 2023.

Table 7: Quantitative 4D reconstruction results on TUM-dynamics.

	Method	Type	Acc Mean↓	Acc Med.↓	Comp Mean↓	Comp Med. \downarrow	NC Mean↑	NC Med.↑
	VGGT	Dense-view	0.050	0.008	0.055	0.017	0.622	0.695
-	CUT3R StreamVGGT	Streaming Streaming	0.105 0.085	0.012 0.011	0.060 0.058	0.007 0.007	0.582 0.617	0.624 0.690

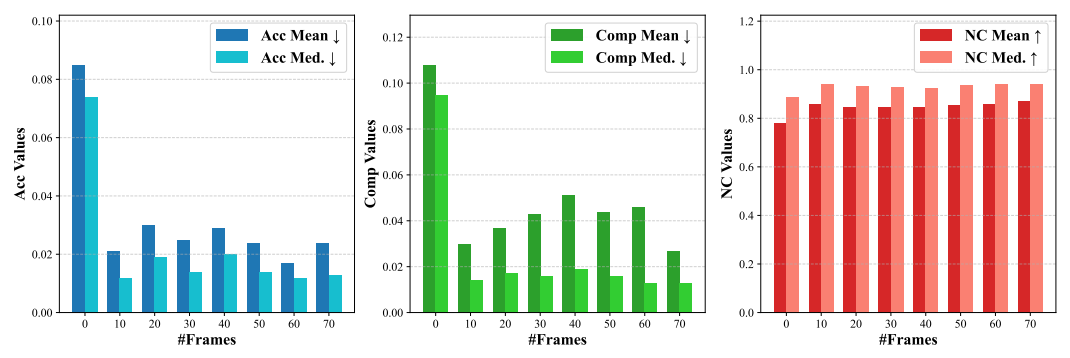


Figure 6: Per-frame results on 7-Scenes (>70 frames).

A APPENDIX

A.1 RECONSTRUCTION PERFORMANCE IN COMPLEX SCENARIOS

It is important to evaluate reconstruction performance of our method under complex scenarios such as long-sequence or dynamic scenes. We now provide comprehensive quantitative results of our method as follows.

Quantitative Reconstruction Performance on the TUM-dynamics Dataset. To evaluate reconstruction performance of our StreamVGGT under dynamic scenarios, we conduct experiments on TUM-dynamics dataset, which contains dynamic object. Specifically, 50 frames are sampled from each sequence for this assessment. Based on these results in Table 7, we believe our method demonstrates strong capability for streaming 4D reconstruction in dynamic scenarios.

Per-frame Metrics on a Long Sequence. To evaluate the temporal coherence of StreamVGGT on long-sequence. We conduct this experiment on the 7-Scenes dataset, each sequence includes over 70 frames. We report the per-frame evaluation metrics at every 10th frame as shown in Figure 6. The results demonstrate that our approach maintains robust temporal consistency.

Loop Closure Analysis. Specifically, for each sequence in the 7-Scenes dataset, we select the first 50 consecutive frames and extend them into a forward-and-reverse order to simulate loop closure scenarios. Then, we evaluate the camera pose errors between the first and last frames (the same frame) for each sequence to assess the performance under loop closure conditions. The results in Table 8 demonstrate that our model achieves lower drift and usable performance in loop closure scenarios.

Quantitative Reconstruction Performance when the Video Stream is Interrupted. It is important for streaming methods to maintain usable performance when the input video stream is interrupted for a period of time. As a result, we provide quantitative reconstruction results of our model on the 7-scenes dataset, where for each sequence we pick the first 50 frames and then remove the middle consecutive 25 frames to simulate the scenarios. The results in Table 9 demonstrate that our model can handle this challenging scenario better than the baseline CUT3R.

A.2 MORE ANALYSIS

Cached Memory Token. To validate the effectiveness of the cached memory token, we evaluated StreamVGGT on the ETH3D (Schops et al., 2017) dataset under two settings: full-sequence input and streaming input, as shown in Table 10. "Time" denotes the inference latency of the final frame in a 40-frame stream. The results indicate that cached memory tokens not only accelerate streaming inference but also preserve temporal consistency and perceptual accuracy.

Table 8: Camera pose estimation on 7-Scenes under loop-closure scenarios.

Method	Type	Avg. Translational Error (m) \downarrow	Avg. Rotational Error (°)↓
CUT3R	Streaming	0.0861	1.39
StreamVGGT	Streaming	0.0080	0.48

Table 9: Results on 7-Scenes when the video stream is interrupted.

Method	Type	Acc Mean↓	Acc Med.↓	Comp Mean↓	Comp Med.↓	NC Mean↑	NC Med.↑
CUT3R	Streaming	0.042	0.024	0.037	0.016	0.702	0.808
StreamVGGT	Streaming	0.036	0.020	0.033	0.012	0.724	0.833

Table 10: Effects of the cached memory token.

Methods	Input Type	Acc.↓	Comp.↓	Overall↓	Time↓
StreamVGGT (W/ Causal Attention)	Full-sequence	0.782	0.723	0.753	4.7 s
StreamVGGT (W/ Cached Token)	Streaming	0.782	0.723	0.753	0.07 s



Figure 7: Visualization of the reconstruction results of StreamVGGT and CUT3R on 7-Scenes.

More Visualizations. Although some of our reconstruction results are presented in the main paper, we provide additional visualizations of the reconstruction outcomes of StreamVGGT and CUT3R on the 7-Scenes dataset. We compare our 3D reconstruction results with CUT3R and the ground truth in Figure 7, which demonstrates that our method achieves high-accuracy 3D reconstruction with fewer outliers and superior spatial consistency.

A.3 DEMO VIDEO & CODE

We include a demo video and our in the supplementary material.

A.4 FURTHER DISCUSSIONS

Limitations. Although our cached token memory mechanism effectively retains historical frame information, this approach leads to a substantial increase in memory usage and computational overhead for long-term sequences as shown in Figure 2. As more frames are processed, the memory footprint grows rapidly due to the accumulation of cached tokens. This scalability issue poses a significant challenge for deploying the model on lightweight or mobile devices, where hardware resources are limited. Therefore, addressing memory efficiency while preserving accuracy remains a critical area for future optimization.

Broader Impacts. The StreamVGGT model offers significantly broader impacts across multiple industries, especially in the domain of low-latency 3D visual geometry reconstruction. By integrating temporal attention with a Cached Token Memory mechanism, StreamVGGT enables efficient incremental processing of multi-view images, ensuring low-latency scene updates with minimal latency while maintaining long-term spatial consistency. This innovative approach makes it a crucial technology for dynamic applications such as autonomous navigation, robotics, and immersive AR/VR experiences, where timely and accurate 3D scene understanding is essential.